ChemElectroChem

Chemistry Europe
European Chemical Societies Publishing

Reprint

WILEY-VCH

Cation-Specific Electrokinetic Separations Using Prussian Blue Intercalation Reactions

Jonathan R. Thompson, Collin D. Davies, Jan Clausmeyer, and Richard M. Crooks*[a]

We report a new approach for forming ion depletion zones (IDZs) using intercalation reactions at an electrochemically controlled Prussian blue (PB) film. The experiments described here were performed using a microfluidic device, wherein a charged fluorophore in solution was used as a proxy to monitor IDZ formation. In the presence of K^+, intercalation reactions proceed readily to form an IDZ, and thus enrich the fluorophore up to 37-fold. In the presence of the larger hydrated Li^+ or tetrabutylammonium (TBA^+) ions, however, ion intercalation proceeded less quickly than with K^+. Slower ion intercalation resulted in a weaker IDZ and correspondingly lower enrichment factors of eight- and six-fold, respectively. These results are significant because they show that PB intercalation reactions selectively form an IDZ. Accordingly, we anticipate that these findings will lead to a better understanding and further interesting applications of intercalation materials like PB for efficient and selective enrichment and separations.

1. Introduction

In the field of separation science, ion depletion zones (IDZs) are important because they can be used to enrich[1–4] and separate[5,6] charged analytes. As discussed later, IDZs can be formed in the presence[7–9] or absence[2,10,11] of membranes. Here, we report an alternative electrochemical method for forming IDZs at specified locations within microfluidic devices. In this case intercalation materials are used to sequester ions from solution thereby forming the IDZ. As shown in Scheme 1a, this is accomplished by controlling the oxidation state of an electroactive intercalation material like Prussian blue (PB). By electrochemically controlling ion motion in and out of PB, the ion concentration in the nearby solution can be actively modified to yield an IDZ.

The use of intercalation materials for establishing IDZs is significant for the following four reasons. First, while intercalation materials like PB have previously been used to sequester cations,[12,13] here we show that the IDZ resulting from intercalation can be used to both separate and concentrate anions that do not intercalate. Second, intercalation materials are often able to discriminate between different ions on the basis of their charge or size. Therefore, an IDZ will only form in the presence of a specific subset of ions that are accommodated by the lattice of the intercalation material. In other words, formation of the IDZ is ion specific. Third, electroactive intercalation materials, like the PB used here, provide a means for exerting electrochemical control over electro-inactive ions like K^+ without producing side products. As we will discuss later, this can be an important factor for establishing and

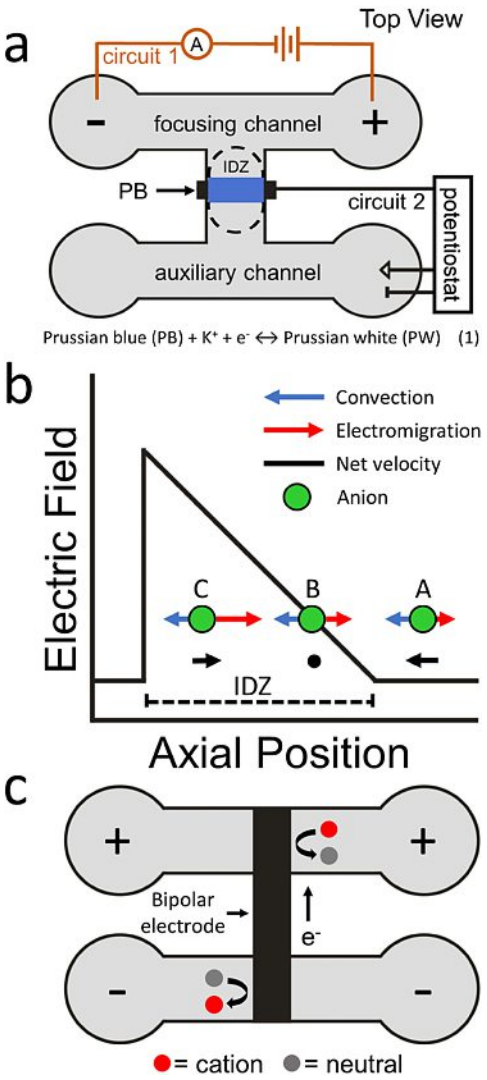

Scheme 1. (a) Schematic illustration of the microelectrochemical device used in this study. (b) Representation of the forces leading to establishment of the IDZ. (c) The electrochemical forces operative in flCP.

[a] J. R. Thompson, Dr. C. D. Davies, Dr. J. Clausmeyer, Prof. R. M. Crooks
Department of Chemistry and Texas Materials Institute
The University of Texas at Austin
105 E. 24th St., Stop A5300, Austin, Texas 78712-1224, United States
E-mail: crooks@cm.utexas.edu

Supporting information for this article is available on the WWW under https://doi.org/10.1002/celc.202001095

controlling an IDZ. Fourth, although this report focuses on PB, the approach described here should be general and applicable to other electroactive intercalation materials that are specific for different classes of ions.

IDZs are formed during a process known as ion concentration polarization (ICP).[14,15] ICP is an electrokinetic phenomenon originating from selective separation of ions, and it is most commonly implemented using nanoporous channels[10,11] or charge-selective membranes like Nafion.[7–9] When a voltage is applied across appropriate channels or membranes, selective ion transport leads to both an IDZ and an ion enrichment zone (IEZ). Because the IDZ is a region of low relative solution conductivity, a disproportionate amount of the applied voltage is dropped within it. This results in a co-located electric field gradient where ions experience enhanced electromigration.

At the location within the IDZ where electromigration is equal and opposite to bulk convection, ions can be focused[8,16] or redirected[17–19] based on device design. This principle is illustrated in Scheme 1b. Here, ions experience uniform bulk convection at every axial position, but electromigration varies as a function of the electric field strength. For example, at point *A* where the electric field is low, convection dominates electromigration and ions move from right to left. As ions flow downstream, electromigration increases with the elevated electric field associated with the IDZ. At point *B*, ions focus because electromigration is equal in magnitude but opposite in direction to bulk convection. Any ions that diffuse downstream to point *C* experience a larger electric field which redirects them back to point *B*. The net effect of this is that ions enrich at point *B*.

There is broad interest in applications that take advantage of ICP. For example, the lowered electrolyte concentration within an IDZ leads to faster electroosmotic flow (EOF), which could improve desalination efficiency during electrodialysis.[20] Additionally, utilizing ICP has gained significant interest for lab-on-a-chip applications, including: separation of charged analytes,[21–23] high-voltage fluidic diodes,[24] manipulation of charged analytes in microdroplets,[9] and microfluidic mixing.[25–27] The electric field gradient associated with ICP has also been used for dielectrophoresis of cells,[14,28,29] salt water desalination,[17,30–32] and analyte enrichment.[33] Analytes such as charged fluorophores,[1,34,35] microparticles,[23,36] and proteins[37,38] have all been enriched, with up to a million-fold enrichment factor in one case.[16]

A few years ago, our group introduced an electrochemical variant of ICP called faradaic ICP (fICP).[39] fICP uses electrochemical reactions to produce an IDZ and accompanying electric field gradient. Specifically, water hydrolysis at the cathodic pole of a bipolar electrode[40–43] neutralizes buffer ions in solution and forms the IDZ (Scheme 1c). We have shown fICP operates like traditional ICP at a nanopore or membrane, and so it is able to separate,[5,6,18] enrich,[2,44] deplete,[45] and control delivery[3,46] of charged analytes in microfluidic devices. fICP also presents some specific advantages over traditional ICP. For example, lithographic fabrication of electrodes is simple, whereas fabrication of nanopores or integration of membrane materials into microfluidic devices can be difficult. Moreover, nanopores and membranes can clog during device operation, a problem that is avoided by using electrodes.

Despite these advantages, fICP suffers from two major limitations. First, as presently implemented, formation of an IDZ requires a buffered solution. Second, the large potential applied to the IDZ-forming electrode may result in undesirable electrogenerated products that counteract IDZ formation.[47] These shortcomings motivated us to explore other electrochemical methods for forming IDZs.

As discussed earlier, the use of ion intercalation processes for forming IDZs offers some significant advantages over fICP. Intercalation materials insert common cations, like K^+ and Na^+, which are electro-inactive in water and thus cannot usually be controlled using fICP. Additionally, intercalation reactions selectively remove small cations that can insert into the lattice of the material, which provides a level of specificity without electrogenerating byproducts. Finally, ion insertion into intercalation materials retains the central advantage of fICP, which is that it can be actively controlled electrochemically. Specifically, the presence or absence of an IDZ depends on the threshold potential of the redox reactions occurring at the controlling electrode. This is in contrast to nearly all membrane-mediated ICP processes, which transport ions to form an IDZ in the presence of any applied electric field.

In the present article, we support these claims by using a charged fluorophore to visualize formation of an IDZ[2,3,5] near a PB-coated working electrode. Additionally, we show that forming the IDZ is cation selective. Specifically, when the cation in solution is K^+, the fluorophore is enriched up to a factor of 37-fold. Bulkier cations, like hydrated Li^+ and tetrabutylammonium (TBA^+) that insert into the PB lattice to a lesser degree, lead to significantly lower enrichment factors of 8- and 6-fold, respectively.

Experimental Section

Chemicals

Reagent grade KCl and HCl were obtained from Fisher Scientific. $FeCl_3 \cdot 6\ H_2O$ (99 + %) and reagent grade $K_3Fe(CN)_6$ were purchased from Acros Organics. $LiClO_4$ (99.9%) was provided by Aldrich. Tetrabutylammonium perchlorate (TBAP) was obtained from GFS Chemicals (Columbus, OH). Fluorescent 4,4-difluoro-1,3,5,7,8-pentamethyl-4-bora-3a,4a-diaza-s-indacene-2,6 disulfonic acid, disodium salt ($BODIPY^{2-}$) was purchased from Molecular Probes (Eugene, OR). Polystyrene microbeads were obtained from Bangs Laboratories (diameter = 0.99 μm, Fishers, IN). All solutions were prepared using deionized water (DI water, > 18.0 MΩ·cm, Milli-Q Gradient System, Millipore, Burlington, MA). Poly(dimethylsiloxane) (PDMS) was prepared using a Sylgard 184 elastomer kit from Dow Silicones Corp. (Midland, MI). All reagents were used as received and without further purification.

Microfluidic Device Fabrication

The hybrid PDMS/quartz microfluidic device was fabricated as previously reported.[48] Briefly, quartz slides were immersed into freshly prepared piranha solution (3:1 H_2SO_4:H_2O_2, *caution: piranha reacts violently with organic materials and solvents*) for 15 min and

then thoroughly rinsed with DI water. Adhesion promoter (Micro Prime HP Primer, Shin-Etsu MicroSi, Phoenix, AZ) and photoresist (AZ 1518, AZ Electronic Materials, Somerville, NH) were spin-coated onto the slides, which were then exposed to UV light through a mask. The photoresist pattern was developed with AZ 400K developer (AZ Electronic Materials). Next, the slides were placed in a tube furnace with a reducing atmosphere (95% N_2/5% H_2, Praxair, Austin, TX), where they were baked at 1000 °C for 1.0 h to form pyrolyzed photoresist film (PPF)[49,50] circuits on the quartz slides.

The PDMS microchannel was fabricated using an elastomer kit and a microchannel mold patterned using SU-8 photoresist (Micro-Chem, Westborough, MA) on a Si wafer. Here, the focusing and auxiliary channels (Scheme 1a) were 10 mm long, 20 μm wide, and they were separated by a 200 μm-wide, 300 μm-long cross channel. The height of all the microchannels was 16.5 μm. Reservoirs, serving as inlets and outlets, were punched into the PDMS using a 4 mm biopsy punch. The quartz slide and the PDMS block were then rinsed with ethanol, dried with N_2, and exposed to an O_2 plasma for 45 s (medium power, 60 W, model PDC-32G, Harrick Scientific, Ithaca, NY). The PDMS and quartz were then brought into contact and baked at 65 °C for 5 min to promote irreversible bonding.

PB Electrosynthesis

PB electrodeposition was performed using slight modifications to a method reported by Karyakin and coworkers.[51] A solution containing 2.0 mM $K_3Fe(CN)_6$, 2.0 mM $FeCl_3$, 100.0 mM KCl, and 100.0 mM HCl was prepared, and 40 μL were placed into the inlet reservoir and 20 μL into the outlet reservoir of the microfluidic channel. The height differential in the reservoirs resulted in pressure-driven flow (PDF) across the working electrode. The working, reference (leak-free Ag/AgCl, eDAQ, Colorado Springs, CO), and counter electrodes were connected to a potentiostat (650C, CH Instruments, Austin, TX), as shown in Scheme 1a. PB was deposited onto the working electrode by cycling the potential of the working electrode from 0.60 V to −0.10 V (all potentials are reported vs. Ag/AgCl) five times at 5.0 mV/s. The PB precursor solution was then removed from the channel and freshly prepared 1.0 M KCl solution was flowed through the device by PDF. Finally, the PB film was electrochemically conditioned by cycling its potential five times from 0.60 V to −0.10 V at 10.0 mV/s (Supporting Information, Figure S1). Optical microscopy indicated that the resulting PB films nearly filled the entire 16.5 μm height of the channel at the leading edge of the working electrode (edge closest to the focusing channel in Scheme 1a). At the trailing edge of the working electrode, the PB film was estimated to be ~5 μm tall.

Ion Concentration Polarization Experiments

The ICP experiments were carried out as follows. First, the microelectrochemical device was flushed with DI water for 10 min, and a solution containing 1.0 mM KCl, 5.0 nM $BODIPY^{2-}$, and 16 fM polystyrene microbeads was added to the inlet and outlet reservoirs. Because the polystyrene microbeads have approximately the same density as water, the motion of the microbeads can be used to measure PDF in the absence of an applied potential.[18,52] The height of liquid in the reservoirs was adjusted so that the linear flow rate across the PB-coated electrode from top-to-bottom was approximately 10 μm/s. Second, 50.0 V was applied to electrodes patterned on the floor of the reservoirs of the focusing channel using a power supply (PWS 4721, Tektronix, Beaverton, OR). The current through the focusing channel was monitored using a Keithley 6517B Electrometer (Cleveland, OH) interfaced with custom LabVIEW software (NI, Austin, TX). Third, IDZ formation was initiated by applying −7.0 V to the PB-coated working electrode using the potentiostat. Note that most of this voltage drops across resistive electrolyte solution along the microchannel length, so only a fraction of it is actually present at the working electrode. During these experiments, the potentiostat was powered by an electrically floating uninterruptable power supply (UPS ES 550, APC, West Kingston, RI). This was necessary to avoid ground loops.

Fluorophore enrichment was observed using an inverted fluorescence microscope (Eclipse TE 2000-U, Nikon, Japan) and a CCD camera (Cascade 512B, Photometrics, Tucson, AZ). The color of the PB thin film was monitored with a top-down optical microscope (Optiphot, Nikon, Japan), and images were obtained using a color CCD camera (Pro 600ES, Pixera, Santa Clara, CA). Image capture and analysis were carried out using V++ (Digital Optics, New Zealand), Viewfinder (Pixera), and ImageJ (NIH, Bethesda, MD) software.

After ICP experiments, the potential of the working electrode was held at 0.80 V for 10 min. This converted the reduced film back to the PB oxidation state. Devices were then rinsed with DI water for 10 min, and the ICP experiments were repeated using solutions containing either 1.0 mM $LiClO_4$ or 1.0 mM TBAP instead of 1.0 mM KCl.

Numerical Simulations

Finite element modeling was carried out using COMSOL Multiphysics software (version 5.5). Simulations were performed on a Dell Precision workstation (Model T7500), which has two Intel Xeon processors (2.40 GHz) and 108 GB of RAM. All simulations were run at steady state. Details of the simulations are provided in the Supporting Information.

2. Results and Discussion

2.1. Device Design and Operation

The goal of this study is to show that intercalation materials can be used to form IDZs that are useful for separating charged analytes. PB was used as the model intercalation material, because it has been extensively studied in the literature[53,54] and can be reversibly cycled many times with little-to-no capacity fade.[55] Upon reduction to Prussian white (PW), PB intercalates cations from solution to maintain electroneutrality within its lattice (Scheme 1a, eq 1).

In previous ICP experiments, the IDZ-forming process (e.g., buffer neutralization at a bipolar electrode[2,39] or selective charge transport through a nanoporous membrane[7–9]) occurred within a high electric field. This resulted in a substantial electric field gradient in the IDZ (Scheme 1b). In the present experiments, however, PB reduction (the IDZ-forming process) must occur within a low electric field. This condition avoids electrocatalytic reduction of water at the PB surface,[56] and the corresponding formation of OH^- which compromises the IDZ and degrades the PB film.[51]

Taking into account the foregoing discussion, we designed the experiment illustrated in Scheme 1a. PB was electrodeposited onto a PPF electrode adjacent to the focusing channel. Circuit 1 (orange) was then used to apply a high electric field across the focusing channel, while a potentiostat in circuit 2 (black) was used to control the oxidation state of the PB film.

Reduction of PB leads to the formation of PW and a corresponding IDZ that propagates into the focusing channel and forms an electric field gradient in solution. Because of the spatial separation of the two electric fields, the voltage applied to the PB-coated electrode in circuit 2 does not significantly affect the expansion of the IDZ into the focusing channel. Importantly, an electrically floating uninterruptable power supply, which minimizes electrical interference between circuits 1 and 2, was used to power the potentiostat.

2.2. Forming an IDZ by Intercalation Reactions

Details of how the ICP experiments were carried out are provided in the Experimental Section. Briefly, however, a solution containing 1.0 mM KCl, 5.0 nM $BODIPY^{2-}$, and 16 fM polystyrene microbeads was placed in the reservoirs of the device to initiate PDF from the focusing channel to the auxiliary channel (Scheme 1a). Next, 50.0 V was applied across the focusing channel. Finally, −7.0 V was applied to the PB-coated electrode to reduce the PB to PW (but note that most of this voltage is dropped in the electrolyte solution).

Figure 1 is a series of fluorescence micrographs showing the results from a typical ICP experiment. The images display the focusing channel immediately adjacent to the PB-coated electrode. Figure 1a shows the device before any voltages were applied, where the $BODIPY^{2-}$ is uniformly distributed in solution. Figure 1b shows the microfluidic device after applying 50.0 V across the focusing channel but prior to reduction of PB. In this case, the $BODIPY^{2-}$ fluorophore remains uniformly distributed within the microfluidic channel. This control experiment demonstrates that the channel geometry, particularly the cross channel (Scheme 1a), does not affect the distribution of $BODIPY^{2-}$ within the focusing channel.

Figures 1c–e show the device at different times after −7.0 V was applied to the PB-coated electrode. Here, $BODIPY^{2-}$ is enriched in the focusing channel just above and to the right of the PB-coated electrode. This indicates that PB reduction, and concomitant K^+ intercalation (eq 1), results in an IDZ that extends into the focusing channel. The corresponding electric field gradient is responsible for enrichment of $BODIPY^{2-}$ (Scheme 1b). Finally, Figure 1f shows the device once PB reduction is terminated (i.e., the PB-coated electrode is set to open circuit). After this occurs, the IDZ and accompanying electric field gradient dissipate and the enriched analyte band disperses. A video showing the entire ~3 min duration of the experiment from which the frames in Figure 1 were extracted is provided in the Supporting Information (Movie S1).

Figure 2 is a plot of the fluorescence intensity of the enriched band within the focusing channel over the duration of the ICP experiment shown in Figure 1. Initially, the fluorescence intensity corresponds to the background value. At $t = 20$ s, corresponding to initiation of PB reduction, there is a steep increase in fluorescence intensity as $BODIPY^{2-}$ begins to enrich. The increase in fluorescence intensity is initially fast because the fluorophore that was distributed within the cross channel is compressed into an enriched band in the focusing channel.

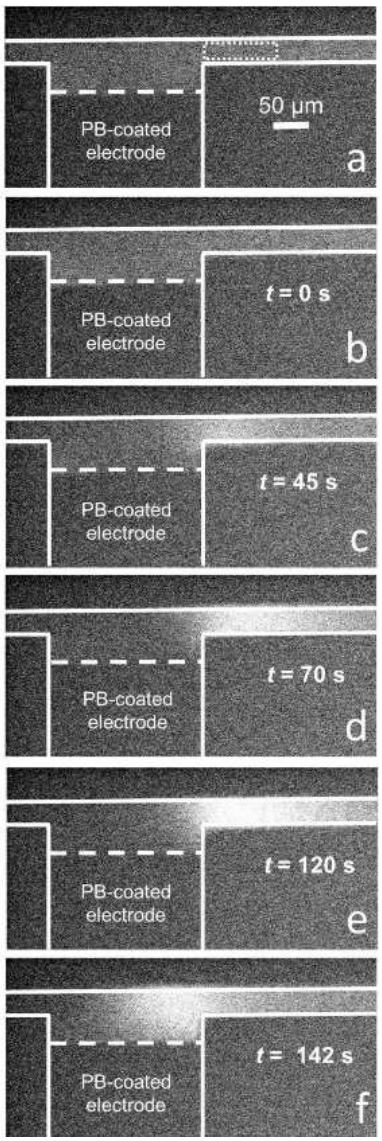

Figure 1. Fluorophore enrichment in the microfluidic device depicted in Scheme 1a. Representative fluorescence micrographs of the focusing channel adjacent to the PB-coated electrode during an ICP experiment at the times indicated within the frames. a) Before applying any voltages. b) After applying 50.0 V across the focusing channel, but while the PB-coated electrode was still at open circuit. c–e) At the times indicated in the frames during the ICP experiment after applying −7.0 V (vs. Ag/AgCl) to the PB-coated electrode. f) 2 s after returning the PB-coated electrode to open circuit potential. The solution contained 1.0 mM KCl, 1.0 μM $BODIPY^{2-}$, and 16 fM polystyrene microbeads. 1.0 μM $BODIPY^{2-}$ was used in this experiment to better visualize fluorophore enrichment. At the start of the experiment, solution flowed from right to left by PDF at a rate of ~10 μm/s. Application of 50.0 V across the focusing channel resulted in EOF from right to left.

Subsequently the fluorescence intensity increases at a slower rate, which corresponds to the rate of transport of the $BODIPY^{2-}$ to the location of enrichment. At $t = \sim 110$ s, the rate of enrichment begins to plateau. Note that because the PB is not fully converted to PW over the course of this experiment (details regarding the PB capacity are provided in the Supporting Information), the extent of fluorophore enrichment is not limited by the PB capacity using this device configuration.

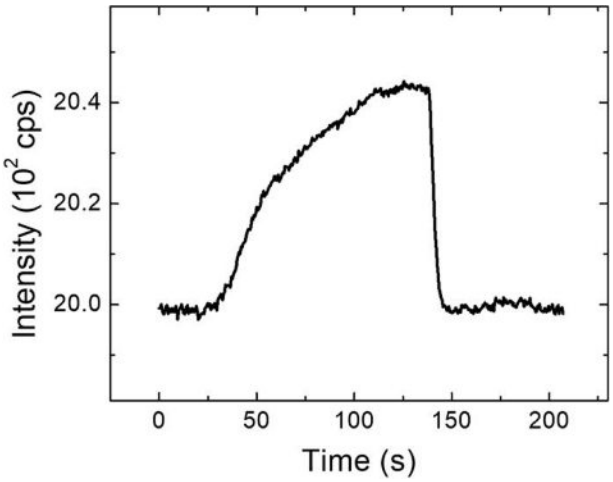

Figure 2. Average fluorescence intensity of the pixels within the region outlined by the dotted white box in Figure 1a as a function of time. The solution contained 1.0 mM KCl, 1.0 μM $BODIPY^{2-}$, and 16 fM polystyrene microbeads. Solution flowed from right to left by PDF at a rate of ~10 μm/s. 50.0 V was applied across the focusing channel and resulted in EOF from right to left. −7.0 V (vs. Ag/AgCl) was applied to the PB-coated electrode from $t = 20$ s to $t = 140$ s.

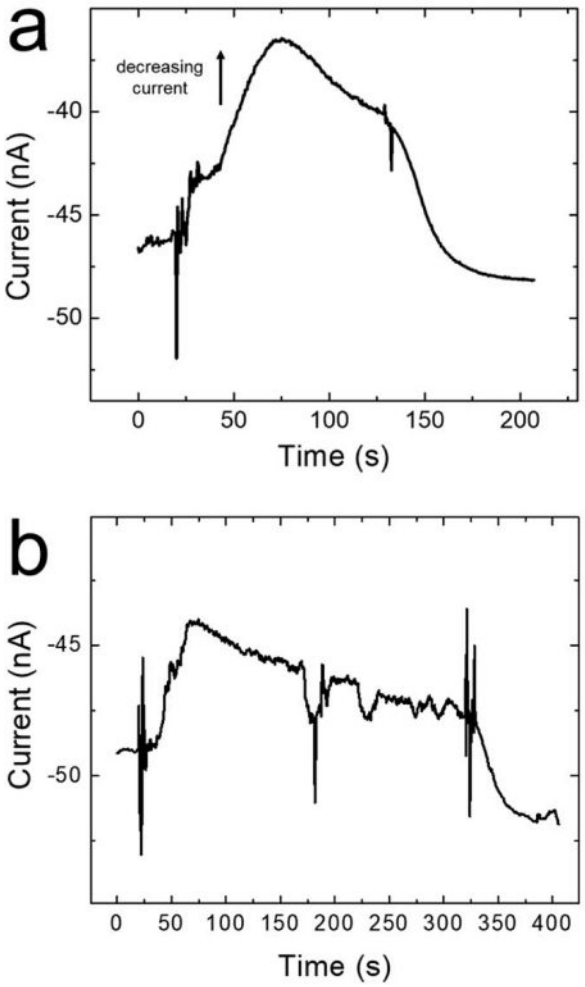

Figure 3. Representative plots of the current passed through the focusing channel as a function of time for both a a) 2 min ICP experiment and a b) 5 min ICP experiment. The solution contained 1.0 mM KCl, 5.0 nM $BODIPY^{2-}$, and 16 fM polystyrene microbeads. 50.0 V was applied across the focusing channel and −7.0 V (vs. Ag/AgCl) was applied to the PB-coated electrode.

Fluorophore enrichment and the enrichment mechanism are discussed in more detail later. Finally, at $t = 140$ s, PB reduction is terminated and the enriched band flows downstream, resulting in the fluorescence intensity returning to the background value.

Figure 3a is a representative plot of the current through the focusing channel during an ICP experiment like the one represented by Figures 1 and 2 (a representative plot of the current through Circuit 2 is also provided in the Supporting Information, Figure S2). Upon application of the 50.0 V driving voltage across the focusing channel ($t = 0$ s), a steady-state current flows. When PB reduction is initiated at $t = 20$ s, the IDZ begins to form and propagate into the focusing channel. In turn, the current passing through the focusing channel decreases because the IDZ raises the total resistance of the fluidic channel. Similar results have previously been reported by our group[52,57] and others[58,59] for related experiments. Notably, this decrease in current, beginning at $t = 20$ s, corresponds to the initiation of $BODIPY^{2-}$ enrichment. $BODIPY^{2-}$ enrichment starts as the IDZ extends into the focusing channel because of the co-located electric field gradient that forms in solution (Scheme 1b).

It is important to note that after the initial decrease, the current begins to rise even while PB is continuously reduced (from $t = \sim 75$ s to 140 s). Similar behavior has been reported previously for an ICP device,[37] and we believe the observed trend results from a similar phenomenon. Specifically, the reduced ion concentration associated with the IDZ results in a localized increase in EOF. Enhanced EOF within the IDZ increases mass transport and causes the rise in current displayed in Figure 3a. This point is discussed in more detail in the Supporting Information.

Finally, when PB reduction is terminated (PB-coated electrode potential moved to open circuit) at $t = 140$ s, the current passing through the focusing channel returns to the initial value as the IDZ dissipates. This timing coincides with the dispersion of the enriched analyte band (Figure 1f, 142 s), further confirming that the observed $BODIPY^{2-}$ enrichment is associated with the IDZ resulting from PB reduction.

Optical microscopy (Figure 4) was performed to directly correlate the formation of the IDZ to ion intercalation (eq 1). These micrographs were obtained under conditions as similar as possible to those in Figures 1–3, but because the optical microscopy required a different microscope, it was not possible to carry them out simultaneously. Figure 4a is an optical micrograph of the PB-coated electrode at $t = 0$ s (before PB reduction). Note that the PB film is darker toward the leading edge of the electrode (the part closest to the focusing channel). This is a consequence of the PB electrodeposition process, which leads to a thickness gradient in the film. The gradient

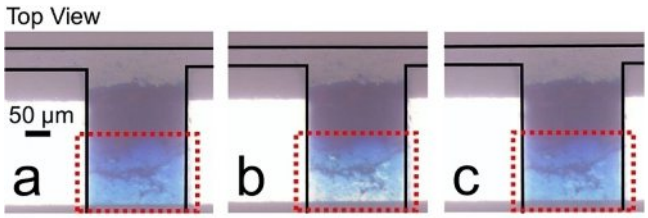

Figure 4. Optical micrographs showing the PB-coated electrode and, at the top of each image, a portion of the focusing channel. The red-dotted box represents the region where the PB is thinnest and the PB color change during the ICP experiment is most apparent. The micrographs were obtained: a) before the ICP experiment, b) 120 s into the ICP experiment, and c) after the ICP experiment was completed and the film was re-oxidized. The solution contained 1.0 mM KCl, 5.0 nM $BODIPY^{2-}$, and 16 fM polystyrene microbeads. 50.0 V was applied across the focusing channel and −7.0 V (vs. Ag/AgCl) was applied to the PB-coated electrode.

occurs due to non-uniform mass transport to the working electrode during electrodeposition. Specifically, convection from the focusing channel to the auxiliary channel (Scheme 1a) results in a higher flux of precursor ions to the leading edge of the electrode than to the trailing edge, thus more PB is deposited at the former than the latter. The main point of this micrograph, however, is to show that the entire PB film is blue before the ICP experiment commences.

As the names suggest, the reduction of PB to PW is accompanied by a color change from blue to white. Indeed, Figure 4b reveals such a color change at the PB-coated electrode at $t = 120$ s during the ICP experiment. This color change is most obvious at the trailing edge of the electrode where the film is thinnest (within the dashed red box). These data prove that PB reduction and IDZ formation occur simultaneously.

Following the ICP experiment, the film was electrochemically oxidized from PW back to PB, and the corresponding color change of the film was monitored. Figure 4c shows that the majority of the PB film reverts to blue and qualitatively demonstrates that most of the film remains intact on the electrode following the ICP experiment. This latter result is important because it shows that the film is not significantly degraded after one round of ICP. Additionally, it suggests that the film can be used to enrich ions multiple times. This point is addressed quantitatively later.

Finally, we performed a control experiment wherein no PB was deposited onto the working electrode of circuit 2 (Scheme 1a). This experiment was carried out to verify that enrichment was a direct consequence of the presence of the PB film and not simply a result of the two electric fields interacting in solution. In this experiment, neither fluorophore enrichment nor a decrease in the current was observed (Supporting Information, Figure S3).

In summary, the foregoing experiments demonstrate that PB intercalation reactions yield a significant IDZ that can be used to enrich ions in solution.

2.3. Effect of Cation and Driving Voltage on Fluorophore Enrichment

The ICP experiments discussed in this section were performed as described in the earlier sections with the following two exceptions. First, the electrolyte solution contained 1.0 mM of either KCl, TBAP, or $LiClO_4$. Importantly, it is known that the identity of the anion has little or no effect on PB intercalation reactions, and therefore the focus here is on differences in cation intercalation.[60–62] Also note that enrichment experiments on replicate devices were performed using the cations in a different order. Specifically, for device 1, enrichment experiments were performed in the following order: K^+, TBA^+, and then Li^+, while for Device 2 the order was TBA^+, Li^+, and then K^+. For Device 3: Li^+, K^+, and then TBA^+. This accounted for possible differences between subsequent experiments on the same device. Second, the driving voltage across the focusing channel was either 20.0 or 50.0 V. PB reduction was initiated as before to form an IDZ and enrich $BODIPY^{2-}$. The enriched $BODIPY^{2-}$ concentration in each experiment was found by comparing the brightest pixel of the micrograph to a calibration curve of known fluorescence intensity vs. fluorophore concentration. The enrichment factor was then calculated by dividing this enriched concentration by the initial $BODIPY^{2-}$ concentration.

Results from these experiments are shown in Table 1. Here, most notably, the enrichment factor varies with the identity of the cation in solution, thereby demonstrating that IDZ formation is cation selective. Specifically, enrichment in the presence of K^+ is significantly higher than that of TBA^+ or Li^+. This is because the Stokes radius of K^+ is smaller than the pore radius of the PB lattice (Table S1, Supporting Information),[63,64] which allows K^+ to readily intercalate into PB. The Stokes radii of TBA^+ and Li^+ are larger than the pores of the PB lattice,[63–66] thereby hindering ion intercalation. Hindered intercalation leads to less ion depletion, correspondingly smaller electric field gradients, and thus lower enrichment factors for TBA^+ and Li^+ compared to K^+. Note, however, that slight enrichment does occur with TBA^+ and Li^+ even though neither should intercalate into the PB lattice. This observation can likely be attributed to vacancies in the PB lattice, which are known to form during electrochemical deposition.[53,54] Such vacancies can

Table 1. Maximum enrichment factor as a function of cation type and driving voltage. The standard deviations represent results from experiments performed using three independent microfluidic devices. The initial concentration of $BODIPY^{2-}$ in each experiment was 5.0 nM.

Focusing channel voltage [V]	K^+	TBA^+	Li^+	Ratio of enrichment factors (K^+:TBA^+:Li^+)
20.0	9 ± 1	4.2 ± 0.7	4.8 ± 0.6	1.00:0.47:0.53
50.0	28 ± 6	5.0 ± 0.9	7 ± 1	1.00:0.18:0.25

lead to relatively large pores in the PB lattice that facilitate ion intercalation.

In addition to the identity of the cation, the driving voltage across the focusing channel also affects enrichment factors. Specifically, Table 1 shows enrichment factors for each of the three cations for driving voltages of 20.0 and 50.0 V. In all cases, the enrichment factor is higher at the higher driving voltage. This type of behavior has been reported previously for both fICP and ICP devices and has been primarily attributed to two physical phenomena.[4,37,39] First, faster convection (i.e., EOF, which dominates convection in this system) and enhanced electromigration both arise from the higher electric field. The increase in these opposing forces (Scheme 1b) compresses the analyte band and leads to higher enrichment factors. Second, faster convection increases mass transport of $BODIPY^{2-}$ from the bulk of solution to the location of enrichment.[4,37]

A subtle takeaway from the data in Table 1 is that differences in solution-phase cation mobility are not responsible for the observed cation-selective enrichment. If cation mobility was responsible, then the ratio of the enrichment factors for K^+, TBA^+, and Li^+ would be the same at both 20.0 and 50.0 V (Table 1). This is because cation mobility is independent of driving voltage.

One final point, fluorophore enrichment is relatively insensitive to experimental parameters. For example, increasing the driving voltage by 2.5-fold results in just a 3.2-fold increase in maximum enrichment factor for K^+. This finding is related to the experimental design and will be discussed in more detail later.

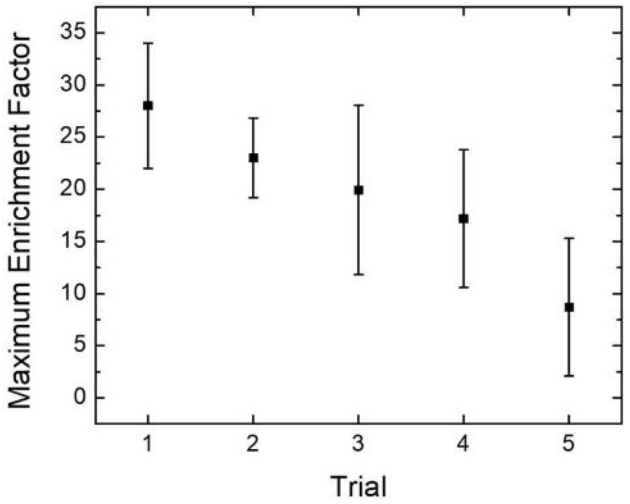

Figure 5. Maximum enrichment factor of $BODIPY^{2-}$ on a single device over the course of five consecutive ICP experiments. The maximum enrichment factor was found by taking the value associated with the brightest pixel during the enrichment experiment and comparing it to a calibration curve of fluorescence intensity vs. known fluorophore concentrations. The error bars represent the standard deviation from the mean for experiments performed on three independent devices. The solution contained 1.0 mM KCl, 5.0 nM $BODIPY^{2-}$, and 16 fM polystyrene microbeads. 50.0 V was applied across the focusing channel and −7.0 V (vs. Ag/AgCl) was applied to the PB-coated electrode.

2.4. Device Capabilities

The degree to which the device can be reused is an important performance metric. In this section, the results of repeated enrichment experiments using a single PB film, as well as longer enrichment times using a single film, are described. Note that up to this point all experiments employed a freshly prepared device and the reduction of the PB film was limited to a maximum of 2 min before converting the film from PW back to PB.

It has previously been shown that PB can be cycled to and from PW (eq 1) at least 30 times with no capacity fade.[55] Accordingly, we performed multiple enrichment experiments consecutively using a single device to determine the stability of the PB film. These ICP experiments were carried out as described for Figure 1. After each enrichment trial, the PB film was held at an oxidizing potential (i.e., 0.80 V vs. Ag/AgCl) to convert PW back to PB. The device was then used again to enrich $BODIPY^{2-}$.

Figure 5 is a plot of maximum enrichment factor vs. the number of experimental trials carried out using a particular film. The results show that repeated enrichment of the $BODIPY^{2-}$ fluorophore using a single PB film is possible, but the extent of enrichment decreases as the film is repeatedly cycled between PB and PW. This downward trend in device performance most likely stems from slight degradation or delamination of the PB film over time. Note, however, that even after five trials using the same film, no visible deterioration was apparent from optical microscopy.

In addition to repeated ICP experiments on a single film, longer ICP experiments were investigated. It is important to note that the total capacity of the PB film intrinsically limits the duration of ICP experiments. That is, once all of the PB is converted to PW, intercalation reactions no longer proceed and ions can no longer be removed from solution to form an IDZ. To quantify this limitation, ICP experiments were performed as described for Figure 1, but reduction of the PB film proceeded for 5 min instead of 2 min (details regarding the PB capacity are in the Supporting Information).

Figure 3b is a representative plot of the current passing through the focusing channel as a function of time for such an experiment. Here, the current trace shows the same trend as Figure 3a, wherein the PB film was reduced for only 2 min. Specifically, the current initially decreased when PB reduction was initiated and the corresponding IDZ began to form (t = 20 s). At t = ~65 s, the current begins to rise even though PB reduction is still ongoing. Again, we hypothesize this gradual increase of current is associated with a localized increase in EOF within the IDZ, which is further discussed in the Supporting information. Finally, at t = 320 s, PB reduction is terminated and the current returns to steady state.

The similarity between Figures 3a and 3b is surprising because we expected that, at sufficiently long times, most of the PB film would convert to PW on the electrode and would facilitate electrocatalytic water reduction.[56] Production of highly mobile OH^- would lead to a sharp increase in the current

passed through the focusing channel.[66] Because no such trend is observed in Figure 3b, it suggests the PW film does not electrocatalytically reduce water to a significant degree under our experimental conditions. This finding agrees with a recent report that states PB analogues are generally poor water reduction catalysts.[67] Thus, Figures 3a and 3b likely show the same trend because the only difference between the experiments is the time of PB reduction.

To better understand the impact of reducing the PB film for 5 min, the PB film was analyzed by optical microscopy. Figure S4 in the Supporting Information is the corresponding optical micrograph, which shows the PB film no longer coats the entire working electrode. The damage to the film likely results from simple delamination of the PB during the 5 min experiment. While the original goal of this experiment was to investigate the impact of the limited capacity of the PB film, the optical microscopy reveals that the PB is unstable over the duration of the 5 min experiment. Therefore, ICP experiments using this device design should be limited to shorter enrichment times for optimal performance.

2.5. Numerical Simulations

The primary aim of the foregoing experiments was to understand how intercalation reactions form an IDZ useful for manipulating ion motion. Here, we use finite element modeling to further investigate the enrichment mechanism within the system illustrated in Scheme 1a. The simulations were performed using a 2-dimensional model comprising a portion of the *xy*-plane of the microelectrochemical device. Figure S5 in the Supporting Information shows the modeled domain, which contains the region of the focusing channel adjacent to the PB-coated electrode (Scheme 1a). Specifically, this domain includes the 60.0 μm of the cross-channel between the PB-coated electrode and the focusing channel, as well as 500.0 μm of the focusing channel on either side of the cross-channel.

A complete discussion of the background theory and the methods used to perform the numerical simulations is included in the Supporting Information. Briefly, however, solution convection was resolved using the Navier-Stokes equation and mass transport was modeled using the Nernst-Planck equation with the electroneutrality condition. EOF was approximated using the Helmholtz-Smoluchowski boundary condition. The electric field in solution was determined using the current passed through the focusing channel after PB reduction was initiated and the IDZ formed during an ICP experiment. We defined K^+ flux as a mass transport-limited process by defining the leading edge of the PB-coated electrode (edge closest to the focusing channel in Scheme 1a) as a boundary where the K^+ concentration was set to 0.

Figure 6a is a simulated plot of the $BODIPY^{2-}$ enrichment factor from an ICP experiment. Here, the enrichment location corresponds to the boundary between the IDZ and bulk solution (Figure 6b), which further confirms that $BODIPY^{2-}$ enrichment occurs due to IDZ formation and a concomitant electric field gradient in solution. It is important to note that

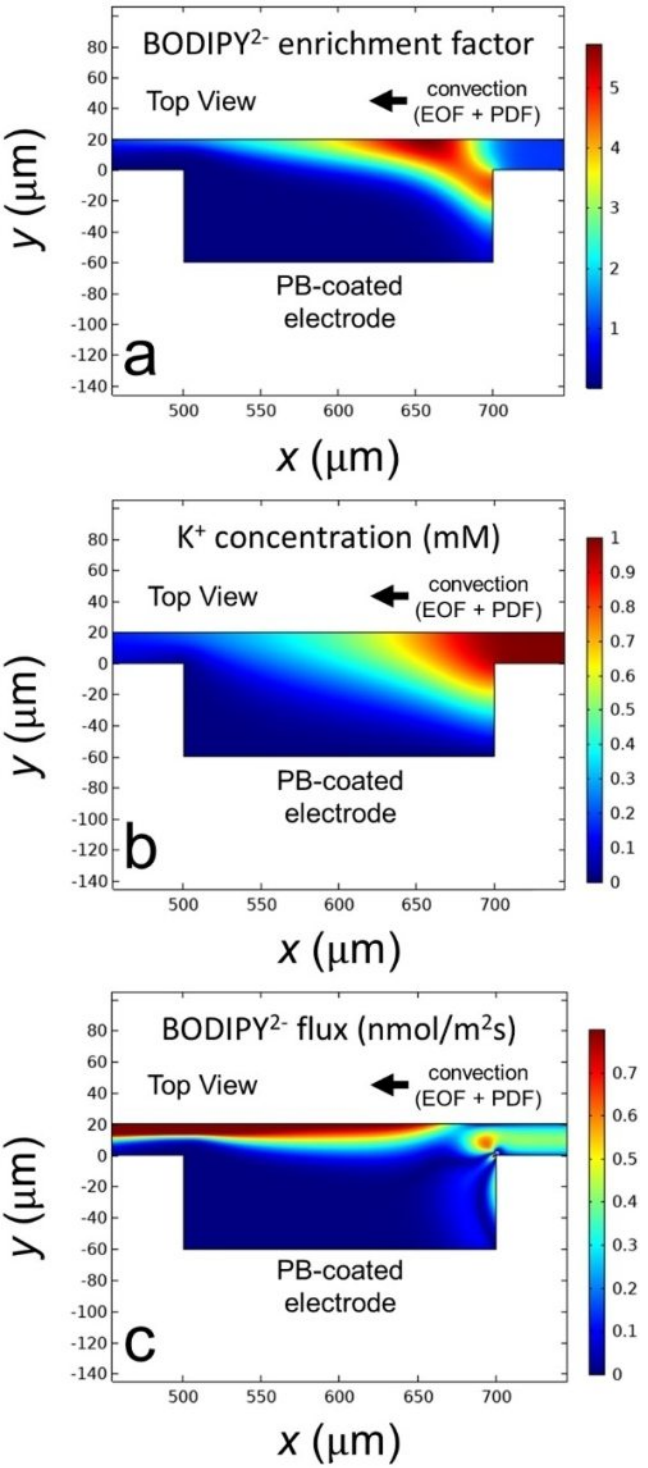

Figure 6. a) Simulated $BODIPY^{2-}$ enrichment factor in the microfluidic device. b) Simulated K^+ concentration after the IDZ propagated from the PB-coated electrode. c) Simulated $BODIPY^{2-}$ flux after the IDZ formed and $BODIPY^{2-}$ was enriched.

the simulated location of $BODIPY^{2-}$ enrichment is in qualitative agreement with the experimental enrichment profile shown in Figure 1. Moreover, while not in quantitative agreement with the experimental results displayed in Table 1, Figure 6a reveals similarly limited $BODIPY^{2-}$ enrichment factors.

To better understand why the experimental degree of enrichment is limited to just a factor of ~30 (Table 1), the simulated flux of $BODIPY^{2-}$ during an ICP experiment was plotted in Figure 6c. Here, a non-uniform flux of $BODIPY^{2-}$ across the width of the focusing channel is apparent. For example, at $x = 675.0$ μm, where $BODIPY^{2-}$ was enriched in the numerical simulations (Figure 6a), the flux of $BODIPY^{2-}$ is higher at $y = 20.0$ μm (0.328 nmol/m^{2}s) than at $y = 0$ (0.085 nmol/m^{2}s). This causes the fluorophore to leak over the 'top' of the IDZ, which in turn leads to the relatively low enrichment factors observed in both the experimental and simulated results.

$BODIPY^{2-}$ leakage occurs for two reasons. First, the device geometry produces asymmetric EOF within the focusing channel from $x = 500.0$ μm to $x = 700.0$ μm (Supporting Information, Figure S6). Specifically, EOF originates from the electrical double layer that forms at the interface between the electrolyte solution and the charged walls of the device. Thus, in the cross channel, the wall at $y = 20.0$ μm gives rise to EOF, leading to faster convection than at $y = 0$ where there is no corresponding wall. This produces asymmetric EOF which contributes to the fluorophore leakage. Second, propagation of the IDZ from the PB-coated electrode results in a non-uniform ionic gradient (Figure 6b) and associated electric field gradient across the width of the focusing channel. Accordingly, electromigration of $BODIPY^{2-}$ varies across the focusing channel further contributing to fluorophore leakage. In other words, variable rates of EOF and $BODIPY^{2-}$ electromigration across the focusing channel differentiate this experiment from the ideal enrichment experiment illustrated in Scheme 1b. In the present case, the forces that contribute to fluorophore enrichment are complex and dynamic, which leads to $BODIPY^{2-}$ leaking past the IDZ, as shown in Figure 6c.

3. Summary and Conclusions

We present two key findings in this report. First, electrochemically controlled PB intercalation reactions can result in an IDZ that is useful for controlling ion motion in solution. This result represents a useful alternative to our previously reported fICP system because intercalation reactions target ubiquitous, electro-inactive ions like K^+. Therefore, fICP in this case is no longer limited to buffered systems. Second, preferential intercalation of K^+ over Li^+ or TBA^+ shows that forming the IDZ is cation specific. Importantly, we anticipate that integrating intercalation materials other than PB would lead to varying degrees of selectivity for forming an IDZ during ICP experiments.

Our results also indicate that the device performance is limited by the stability and finite capacity of the PB film. To improve the capabilities of the device, we plan to incorporate alternative classes of intercalation materials, like layered oxides and polyanionic compounds, that offer higher energy densities and better stability than PB.[68] Additionally, we intend to alter the device design to increase the intercalation-material-surface-area-to-focusing-channel-volume ratio. This will allow the IDZ to form and expand into the focusing channel more effectively, enhancing the resulting enrichment factors. The results of these experiments will be reported in due course.

The foregoing findings are important because they demonstrate a new, ion-dependent approach for selectively forming IDZs. We believe that the results reported here will improve the understanding of both ICP and intercalation processes, while they also represent the first step toward integrating and using intercalation materials for efficient and selective enrichment and separations.

Acknowledgements

We gratefully acknowledge support from the Chemical Sciences, Geosciences, and Biosciences Division, Office of Basic Energy Sciences, Office of Science, U.S. Department of Energy (Grant: DE-FG02-06ER15758). We thank the Robert A. Welch Foundation (Grant F-0032) for sustained support of our research program. We gratefully acknowledge the Center for Electrochemistry at The University of Texas at Austin for access to modeling software and computational resources. J.C. gratefully acknowledges a RURS Gateway fellowship.

Conflict of Interest

The authors declare no conflict of interest.

Keywords: electrochemistry · electrophoresis · intercalation materials · ion concentration polarization · microfluidics

[1] J. Dai, T. Ito, L. Sun, R. M. Crooks, *J. Am. Chem. Soc.* **2003**, *125*, 13026–13027.
[2] R. Dhopeshwarkar, D. Hlushkou, M. Nguyen, U. Tallarek, R. M. Crooks, *J. Am. Chem. Soc.* **2008**, *130*, 10480–10481.
[3] R. K. Perdue, D. R. Laws, D. Hlushkou, U. Tallarek, R. M. Crooks, *Anal. Chem.* **2009**, *81*, 10149–10155.
[4] R. K. Anand, E. Sheridan, D. Hlushkou, U. Tallarek, R. M. Crooks, *Lab Chip* **2010**, *11*, 518–527.
[5] D. R. Laws, D. Hlushkou, R. K. Perdue, U. Tallarek, R. M. Crooks, *Anal. Chem.* **2009**, *81*, 8923–8929.
[6] K. N. Knust, E. Sheridan, R. K. Anand, R. M. Crooks, *Lab Chip* **2012**, *12*, 4107–4114.
[7] R. Kwak, S. J. Kim, J. Han, *Anal. Chem.* **2011**, *83*, 7348–7355.
[8] S. H. Ko, Y.-A. Song, S. J. Kim, M. Kim, J. Han, K. H. Kang, *Lab Chip* **2012**, *12*, 4472–4482.
[9] S. Kim, B. Ganapathysubramanian, R. K. Anand, *J. Am. Chem. Soc.* **2020**, *142*, 3196–3204.
[10] S. J. Kim, Y.-C. Wang, J. H. Lee, H. Jang, J. Han, *Phys. Rev. Lett.* **2007**, *99*, 044501.
[11] A. Mani, T. A. Zangle, J. G. Santiago, *Langmuir* **2009**, *25*, 3898–3908.
[12] F. Yu, L. Wang, Y. Wang, X. Shen, Y. Cheng, J. Ma, *J. Mater. Chem. A* **2019**, *7*, 15999–16027.
[13] Z.-Q. Li, M.-Y. Wu, X.-L. Ding, Z.-Q. Wu, X.-H. Xia, *Anal. Chem.* **2020**, *92*, 9172–9178.
[14] M. Li, R. K. Anand, *Analyst* **2016**, *141*, 3496–3510.
[15] S. J. Kim, Y.-A. Song, J. Han, *Chem. Soc. Rev.* **2010**, *39*, 912–922.
[16] Y.-C. Wang, A. L. Stevens, J. Han, *Anal. Chem.* **2005**, *77*, 4293–4299.
[17] S. J. Kim, S. H. Ko, K. H. Kang, J. Han, *Nat. Nanotechnol.* **2010**, *5*, 297–301.
[18] C. D. Davies, E. Yoon, R. M. Crooks, *ChemElectroChem* **2018**, *5*, 877–884.
[19] C. D. Davies, R. M. Crooks, *Chem. Sci.* **2020**, *11*, 5547–5558.
[20] V. V. Nikonenko, A. V. Kovalenko, M. K. Urtenov, N. D. Pismenskaya, J. Han, P. Sistat, G. Pourcelly, *Desalination* **2014**, *342*, 85–106.

[21] L. Gong, Z. Li, J. Han, *Sep. Purif. Technol.* **2019**, *217*, 174–182.
[22] H. Jeon, H. Lee, K. H. Kang, G. Lim, *Sci. Rep.* **2013**, *3*, 1–7.
[23] S. I. Han, D. Lee, H. Kim, Y. K. Yoo, C. Kim, J. Lee, K. H. Kim, H. Kim, D. Lee, K. S. Hwang, D. S. Yoon, J. H. Lee, *Anal. Chem.* **2019**, *91*, 10744–10749.
[24] R. Kwak, J. Han, *J. Phys. Chem. Lett.* **2018**, *9*, 2991–2999.
[25] T.-C. Kuo, H.-K. Kim, D. M. Cannon, M. A. Shannon, J. V. Sweedler, P. W. Bohn, *Angew. Chem. Int. Ed.* **2004**, *43*, 1862–1865; *Angew. Chem.* **2004**, *116*, 1898–1901.
[26] H. Chun, H. C. Kim, T. D. Chung, *Lab Chip* **2008**, *8*, 764–771.
[27] I. Rubinstein, B. Zaltzman, *J. Fluid Mech.* **2013**, *728*, 239–278.
[28] R. K. Anand, E. S. Johnson, D. T. Chiu, *J. Am. Chem. Soc.* **2015**, *137*, 776–783.
[29] M. Li, R. K. Anand, *J. Am. Chem. Soc.* **2017**, *139*, 8950–8959.
[30] B. D. MacDonald, M. M. Gong, P. Zhang, D. Sinton, *Lab Chip* **2014**, *14*, 681–685.
[31] R. Kwak, V. S. Pham, B. Kim, L. Chen, J. Han, *Sci. Rep.* **2016**, *6*, 25349.
[32] B. Kim, R. Kwak, H. J. Kwon, V. S. Pham, M. Kim, B. Al-Anzi, G. Lim, J. Han, *Sci. Rep.* **2016**, *6*, 31850.
[33] C. Zhao, Z. Ge, C. Yang, *Micromachines* **2017**, *8*, 28.
[34] D.-T. Phan, S. A. M. Shaegh, C. Yang, N.-T. Nguyen, *Sens. Actuators B* **2016**, *222*, 735–740.
[35] V. A. Papadimitriou, L. I. Segerink, J. C. T. Eijkel, *Lab Chip* **2019**, *19*, 3238–3248.
[36] S. Baek, J. Choi, S. Y. Son, J. Kim, S. Hong, H. C. Kim, J.-H. Chae, H. Lee, S. J. Kim, *Lab Chip* **2019**, *19*, 3190–3199.
[37] R. Kwak, J. Y. Kang, T. S. Kim, *Anal. Chem.* **2016**, *88*, 988–996.
[38] S. I. Han, K. S. Hwang, R. Kwak, J. H. Lee, *Lab Chip* **2016**, *16*, 2219–2227.
[39] R. K. Anand, E. Sheridan, K. N. Knust, R. M. Crooks, *Anal. Chem.* **2011**, *83*, 2351–2358.
[40] F. Mavré, R. K. Anand, D. R. Laws, K.-F. Chow, B.-Y. Chang, J. A. Crooks, R. M. Crooks, *Anal. Chem.* **2010**, *82*, 8766–8774.
[41] S. E. Fosdick, K. N. Knust, K. Scida, R. M. Crooks, *Angew. Chem. Int. Ed.* **2013**, *52*, 10438–10456; *Angew. Chem.* **2013**, *125*, 10632–10651.
[42] G. Loget, D. Zigah, L. Bouffier, N. Sojic, A. Kuhn, *Acc. Chem. Res.* **2013**, *29*, 2513–2523.
[43] J. P. Guerrette, S. M. Oja, B. Zhang, *Anal. Chem.* **2012**, *84*, 1609–1616.
[44] E. Sheridan, D. Hlushkou, K. N. Knust, U. Tallarek, R. M. Crooks, *Anal. Chem.* **2012**, *84*, 7393–7399.
[45] E. Sheridan, K. N. Knust, R. M. Crooks, *Analyst* **2011**, *136*, 4134–4137.
[46] K. Scida, E. Sheridan, R. M. Crooks, *Lab Chip* **2013**, *13*, 2292–2299.
[47] C. D. Davies, S. E. Johnson, R. M. Crooks, *ChemElectroChem* **2019**, *6*, 4867–4876.
[48] D. C. Duffy, J. C. Mcdonald, O. J. A. Schueller, G. M. Whitesides, *Anal. Chem.* **1998**, *70*, 4974–4984.
[49] S. Ranganathan, R. L. McCreery, *Anal. Chem.* **2001**, *73*, 893–900.
[50] T. E. Benavidez, R. Martinez-Duarte, C. D. Garcia, *Anal. Methods* **2016**, *8*, 4163–4176.
[51] A. A. Karyakin, E. E. Karyakina, L. Gorton, *Electrochem. Commun.* **1999**, *1*, 78–82.
[52] E. Yoon, C. D. Davies, T. A. Hooper, R. M. Crooks, *Lab Chip* **2017**, *17*, 2491–2499.
[53] K. Itaya, I. Uchida, V. D. Neff, *Acc. Chem. Res.* **1986**, *19*, 162–168.
[54] K. Hurlbutt, S. Wheeler, I. Capone, M. Pasta, *Joule* **2018**, *2*, 1950–1960.
[55] Y. Lu, L. Wang, J. Cheng, J. B. Goodenough, *Chem. Commun.* **2012**, *48*, 6544–6546.
[56] T. Abe, F. Taguchi, S. Tokita, M. Kaneko, *J. Mol. Catal. A* **1997**, *126*, L89–L92.
[57] E. Sheridan, D. Hlushkou, R. K. Anand, D. R. Laws, U. Tallarek, R. M. Crooks, *Anal. Chem.* **2011**, *83*, 6746–6753.
[58] S. M. Rubinstein, G. Manukyan, A. Staicu, I. Rubinstein, B. Zaltzman, R. G. H. Lammertink, F. Mugele, M. Wessling, *Phys. Rev. Lett.* **2008**, *101*, 236101.
[59] H. Lee, D. Kim, J. Y. Kang, K. W. Bong, S. H. Lee, R. Kwak, *Desalination* **2019**, *458*, 14–24.
[60] D. Ellis, M. Eckhoff, V. D. Neff, *J. Phys. Chem.* **1981**, *85*, 1225–1231.
[61] C. A. Lundgren, R. W. Murray, *Inorg. Chem.* **1988**, *27*, 933–939.
[62] J. W. McCargar, V. D. Neff, *J. Phys. Chem.* **1988**, *92*, 3598–3604.
[63] W. Jin, A. Toutianoush, M. Pyrasch, J. Schnepf, H. Gottschalk, W. Rammensee, B. Tieke, *J. Phys. Chem. B* **2003**, *107*, 12062–12070.
[64] M. Pyrasch, A. Toutianoush, W. Jin, J. Schnepf, B. Tieke, *Chem. Mater.* **2003**, *15*, 245–254.
[65] E. R. Nightingale, *J. Phys. Chem.* **1959**, *63*, 1381–1387.
[66] A. J. Bard, L. R. Faulkner, *Electrochemical Methods: Fundamentals and Applications*, Wiley, Hoboken, NJ **2001**.
[67] E. P. Alsac, *Master of Science Thesis*, Bilkent University, **2017**.
[68] K. Chayambuka, G. Mulder, D. L. Danilov, P. H. L. Notten, *Adv. Energy Mater.* **2018**, *8*, 1800079.

Manuscript received: August 19, 2020
Revised manuscript received: September 22, 2020